

Deep Convolutional Neural Network for Skin Lesion Detection with HOG and GLCM features

S. Anisha Thangakani¹, M. Sornam^{*}, Muthusubash Kavitha²

¹Department of Computer Science, University of Madras, Chennai 600025, India

²Graduate School of Advanced Science and Engineering², Hiroshima University, Japan

Received: 29 April 2021

Accepted: 6 May 2021

Published online: 23 February 2022

Keywords: Skin lesion, HOG, GLCM, CNN, classification

Lesion relates to the unnatural growth of tissues in which skin lesions are most common. It may have two types: benign and malignant. Malignant lesion has the highest death rate compared to benign lesion due to their major metastases. Metastasis is nothing but the capacity to enter distant organs. There are a variety of diagnostic features to differentiate both. The most popular approach is the histological approach through which the impacted tissues are taken and examined underneath a microscope. As it is an invasive technique and the chances of spreading to other natural underlying structures, other diagnostic approaches have come into play. This work is one of them, which is a non-invasive technique and is detected by a computer vision algorithm. To determine where such a lesion is malignant or benign, the extraction feature utilizes a mixture of both the Histograms of oriented gradients (HOG) and the Grayscale Level Co-occurrence Matrix (GLCM) functions. Which are applied to the Convolutional neural network. Convolutional neural network (CNN) obtained an average accuracy of 98.32 percent on a dataset of 4100 images, which is greater than the existing method.

© (2022) Society for Biomaterials & Artificial Organs #20058022

Introduction

The skin is the body's largest organ. Humans are most commonly affected by cancer of the skin. Every year, more than 3 million people around the world [1] are diagnosed with some form of skin cancer. Cancer evolves when normal cells undergo an irregular transformation and spread without normal control. The mass known as a lesion is formed as the cells multiply.

Body lesion is also known as cancers of the skin. Only when the lesion consists of malignant cells are said to be cancerous. This implies, due to their uncontrolled growth, that they invade and invade neighboring tissues. The bloodstream or lymph system may also cause lesions to migrate to remote organs. This invasion process is called metastasis and spreads to other organs. Lesions submerge the around tissues by bringing oxygen and nutrients into their space that ordinary cells need to live and work. The 3 primary types of skin cancer are: basal cell carcinoma (BCC), Squamous cell carcinoma (SCC) and melanoma. The vast majority of cancers of the skin are basal cell carcinoma (BCC) or Squamous cell carcinoma (SCC). While malignant, it is unlikely that they would

spread to other bodily areas. If it is not treated early, you will disfigure locally. A small but large number of skin cancers [2] are malignant melanomas. Malignant is a particularly aggressive cancer that tends relatively early and easily to metastasize and spread to other parts of the body. These cancers can be fatal if detected and treatment is not made early.

In existing work, they have used the ABCD (A: asymmetry, B: border, C: colour, and D: diameter) rule with the convolutional neural network but the work does not give a more accurate result. So that we used the Histograms of oriented gradients (HOG) and *Grayscale Level Co-occurrence Matrix (GLCM)* feature to accurately predict whether the lesion is malignant or benign, with the help of a convolutional neural network as a classifier and also explained some of the advantages of the Histograms of oriented gradients (HOG) and *Grayscale Level Co-occurrence Matrix (GLCM)* feature below:

Computation of HOG features: Texture is one of the most important parameters for the detection of medical images. It identifies objects and the region of interest (ROI) for different types of images. Computer image analysis needs to classify, detect and segment based on intensity and colour. The texture analysis was the process of extracting features from the enhanced image using a specific method. Image texture is an entity that consists of

^{*} Corresponding author

madasany.sornam@gmail.com (Dr. M. Sornam, Department of Computer Science, University of Madras, Chennai 600025, India)

pixels or groups of pixels that are related to each other. Histogram of oriented gradients (HOG) is a global descriptor. Based on the distribution of the intensity gradients or the direction of the edge, the shape and appearance of the image are described using the numerical value of the pixel or the amount of light. The gradient is the analyzing different aspects in the intensity or colour of the pixel and is used to retrieve relevant information from an image. The main steps for the calculation of the HOG (Histograms of oriented gradients) features can be described as follows:

1. Computation of image gradient values.
2. Histograms of oriented gradients (HOG) computation called orientation binning. This involves the creation of cell histograms.
3. Histograms of oriented gradients (HOG) computing is the development of descriptor blocks.
4. Histograms of oriented gradients (HOG) computing is a block normalization operation.

Computation of GLCM features: Gray Level Co-occurrence Matrix [1] (GLCM) and associated texture feature computations are techniques for image analysis. Given an image consisting of pixels each with an intensity (a specific grey level), the Gray Level Co-occurrence Matrix is a tabulation of how many other different combinations of grey levels co-occur in an image or an image section. The texture feature computations use the contents of the Gray Level Co-occurrence Matrix to estimate the variation in the intensity of the pixel of interest. Echo view offers a *Grayscale Level Co-occurrence Matrix (GLCM)* Texture Feature operator that produces a virtual variable that represents a texture calculation for a single beam echogram. In this, we're going to measure the selected features. This measurement only utilizes the values in the Gray Level Co-occurrence Matrix Features: Energy, Entropy, Contrast, Homogeneity, and Correlation.

Talha Akram et al. come up with a novel framework for the classification of skin lesions, which integrates in-depth feature information to generate the most discriminating feature vector, with the advantage of preserving the original feature space. Authors use recent deep models for the extraction of features and by taking advantage of the transfer of learning [3]. Initially, the dermoscopic images are segmented and the lesion region is extracted, which is later subjected to the retraining of the selected deep models to generate the fused feature vectors. In the second phase, a framework for the most discriminatory selection and reduction of dimensions is proposed, an entropy-controlled analysis of the neighbourhood component (ECNCA). This hierarchical framework optimizes the fused features by selecting the main components and removing redundant and irrelevant data. The efficiency of our architecture is validated by four benchmark dermoscopic datasets: PH2, ISIC MSK, ISIC UDA and ISBI-2017. The simulation results clearly show that the design is accurate enough to categorize the skin lesion with 98.8 percent, 99.2 percent, and 97.1 percent, and 95.9 percent accuracy with the selected classifiers on all four datasets and with less than 3 percent accuracy.

Aishwariya Dutta et al propose a flexible and fully automated framework for Skin Lesion Classification (SLC) in which they have integrated Image Enhancement, Deep Convolutional Neural Network (DCNN), and Transfer Learning [4]. The proposed framework has been trained and tested on the publicly accessible IEEE International Symposium on Biomedical Imaging (ISBI)-2017 dataset. The average size achieved under the Receiver Operating Characteristic Curve (AUC), recall, precision, and F1-score are 0.87, 0.73, 0.76, and 0.74 respectively for the SLC. Our experimental studies for the classification of lesions show that the proposed

approach can successfully distinguish between high-precision skin cancers, which can identify skin lesions for the recognition of melanoma. Singh Rashi et al. proposed the use of machine learning for Skin Texture Analysis. The analysis proposed includes the acquisition of skin pictures. The 197 input pictures set are used for training and research. The skin images [5] were collected from various fields by the typical dermatologist in the 1 to 10 range and graded as natural good or bad skin. The training phase involves 70 % of the total pictures and the remaining 30% is tested. It is around 99.38 percent accurate to separate pictures into better, negative, and regular skin. Priyadarshini et al.'s method identified for texture analysis is Local Binary Pattern (LBP). A strong extraction feature for texture was found. The help classification vector [6] has achieved sensitivity greater than 97% and specificity greater than 93%, estimated that when LBP [5] is combined with the Histograms of oriented gradients (HOG) classification to increase the detection efficiency of some data sets. In the Bayesian decision to improve melanoma detection rates, Maen Takruri et al. [7] proposed a combination of several classifieds. Results with improved recognition accuracy for the standalone classification of skin lesions demonstrated a comparable confidence interval and a stable recognition rate. In contrast to the standalone Skin Lesion categorizers, the proposed fusion method of the Bayesian decision demonstrates an improved recognition precision. Varma et al. [8] detect identified skin area, intending to divide the picture into the skin and the non-skin pixel, detects the presence of skin detection. The pixels are known as the skin distribution. The combined strategy calls for a multilevel classification. There are several features at each level. The identification of skin pixels is based on both versions. For that colour space, the skin classifier sets the threshold. The performance of the system has been evaluated with accuracy, the F-Score, true positive rates, and the false-positive rate.

For a deep-learning skin diagnosis, Sherin et al. [9] were named. It includes the associated increase portion in segmentation for the role of infected skin injuries and is intended as a feature extractor by the Convolution Neural Network (CNN). A model classifier was modeled on a multi-class SVM, constructed from a digital Skin image dataset, based on *Convolutional neural network* features. The results indicate that all patients with Melanoma and Eczema disease are identified by the proposed procedure. And all patients with skin cancer should be properly determined to be able to detect non-melanoma disease. In the end, the greatest specificity compared to any cancer is melanoma skin cancer.

The detection of skin diseases was established as an important image classification task by Seema et al. [10] The *Convolutional neural network* is a classifier. The *Convolutional neural network* is a classifier. Computer-aided diagnostics are also used for precise and objective accuracy. In various image recognition tasks, deep learning has recently been used. The paper's results indicate that the identity of skin disease is possible through *Convolutional neural network*. The convolution network was used as a classifying system to detect skin diseases from the picture. The overall accuracy is 95%, which shows that, for the stated reason, *Convolutional neural network* is used effectively.

Materials and Methods

Existing method

To further distinguish between the different lesion, the characteristics of the ABCD rule for melanoma (A: asymmetry, B: border, C: colour, and D: diameter) is defined. The rule is based on dermatological principles: shape, colour, and symmetry. The ABCD parameter [11] highlighted additional diagnostic approaches, including automatic analysis of colour images by computerized

image processing, which would make the clinical diagnosis of melanoma easier. As a result, computer-aided systems for the clinical diagnosis of melanoma have become more and more interested as help to dermatologists during various research phases, such as the detection of borderline lesions, extraction of ABCD (A: asymmetry, B: border, C: colour, and D: diameter) parameters, and classification into different types of lesions. However, with the Convolutional neural Network, their functionality was complicated and not very good.

Dataset description

The International Skin Imaging Collaboration (ISIC) is an international attempt to improve the diagnosis of melanoma funded by the International Society for Digital Skin Imaging (ISDIS). The ISIC Archive represents the largest publicly available collection of reliability dermoscopic images of skin lesions.

Currently, the ISIC (International Skin Imaging Collaboration) Archive contains more than 13,000 dermoscopic images that have been collected from leading international clinical centres and acquired from a variety of devices within each centre. The broad and international participation in the Image Contribution is designed to ensure a representative clinically relevant sample. From this ISIC dataset, we have taken 4100 images for the feature extraction of both the Histograms of oriented gradients (HOG) and *Grayscale Level Co-occurrence Matrix (GLCM)* features to extract the features accurately and also trained the 2600 images for classification and 1,550 images for testing purposes.

Proposed method

The proposed system is to distinguish benign and malignant skin lesion images using the ISIC (International Skin Imaging Collaboration) data set [12]. International Skin Imaging Collaboration has developed a benchmark dataset of dermoscopic skin lesions images that are actively available. It explains major challenges, problems in the segmentation of lesions, detection of clinical diagnostic patterns, and classification of lesions, along with a high-resolution human validated training and testing set of nearly 3000 CC-0 licensed images by integrating both the Histograms of oriented gradients (HOG) and *Grayscale Level Co-occurrence Matrix (GLCM)* extraction methods and comparing them with the Convolutional Neural Network.

Preprocessing

Just before images are being segmented, the effectiveness of the segmentation algorithm must be pre-processed and cleaned. The image will then become a grayscale image. The homomorphism filter when Fourier fast transformation has an image, which goes further through the high-pass filter [13]. In a Gaussian image, a Gaussian blur is used. This is labeled the two-dimensional model of Weierstrass [14]. The bokeh effect used to reproduce a circle is more accurate by comparison. Since the mathematician model of Fourier is another mathematician using a mathematician blur, it reduces the high-frequency components of the picture and therefore helps a mathematician blur to remove the presence, by smoothing, of salt and pepper.

Segmentation

The cleaned image was further segmented into the global threshold algorithm Otsu [15]. The Otsu algorithm separates the background image from the foreground image by trying to set the images above the values obtained. The Otsu algorithm enables us to create a grey image histogram before to actually trying to run an algorithm for segmentation. Otsu's algorithm aim is to display a high dimensional

variance threshold value [14] and to define two classes as the weighted sum of variance as in equation 1,

$$\sigma_{\omega}^2 = \omega_0(t)\sigma_0^2(t) + \omega_1(t)\sigma_1^2(t) \quad (1)$$

The probabilities that weights symbol ω_0 and ω_1 are denoted as a threshold value and σ_0^2 , σ_1^2 are denoted as variations in the two classes. The image is then finished and the morphological process is performed above the threshold value.

Feature extraction

After the process of segmenting the image, the process of extraction of the features is carried to identify the acquired segmented skin lesion. In this device [16] we extract the features of Histograms of oriented gradients (HOG) and *Grayscale Level Co-occurrence Matrix (GLCM)*.

HOG features

Image gradient values: Detector performance is suitable to the way in which gradients are computed, but the easiest scheme turns out to be the best.. We tested gradients computed [17] using Gaussian smoothing followed by a few discrete derivative masks. Input image (I) filtered vertically and horizontally as in equations 2 and 3.

$$d_x = [-1, 0, 1] \quad (2)$$

$$d_y = [-1, 0, 1]^T \quad (3)$$

The use of larger masks always seems to reduce performance, and it is significantly damaged by smoothing: Gaussian derivatives d_x and d_y of the grayscale image I or a convolution operation is then obtained for the silhouette as in equation 4, 5.

$$I_x = I * d_x \quad (4)$$

$$I_y = I * d_y \quad (5)$$

The gradient (I) of magnitude and orientation is calculated using the following as in equation 6,7.

$$G =$$

$$\theta = \arctan(I_x/I_y) \quad (7)$$

Probably because the orientation estimation suffers as a result of the x and y filters being installed in different centres. For colour images, we calculate separate gradients for each colour channel and use the one with the highest standard as the pixel gradient vector.

Orientation binning: The next step is the descriptor's fundamental nonlinearity. Based on the orientation of the gradient element centred on it, each pixel calculates a weighted vote for an edge orientation histogram channel, and the votes are accumulated in the orientation bins over the local spatial regions that we call the cell. The cells may be either rectangular or radial (log-polar sectors). The orientation bins are evenly spaced between 0 and 180 ('unsigned' gradient) or 0 to 360 ('signed' gradient). To reduce dimensionality, votes are interpolated bilinear between adjacent bin centres in both orientation and position. Voting is a function of the gradient magnitude at the pixel, either the magnitude itself, its square, its square root, or the clipped shape of the magnitude representing the soft presence/absence of the edge at the pixel. In practice, using the magnitude alone gives more accurate results. If the square root is slightly reduced by using the binary margin balance, the turnout decreases significantly. Fine orientation programming turns out to be vital for quality performance, while (see below)

spatial binning may be rather rough. Increasing the number of orientation bins significantly improves performance up to about 9 bins, but makes little difference beyond that. This is for bins spaced over 0 to 180, i.e. the 'sign' of the gradient is ignored. Including the signed gradients (orientation range 0 to 360, as in the original SIFT (scale-invariant feature transform) descriptor), the performance decreases even when the number of bins is also doubled to preserve the original orientation resolution. In the case of a skin lesion, the wide range of lesion size, depth, and background colours is likely to render the signs of contrasts uninformative.

Descriptor blocks: Gradient strengths vary across a wide range due to local variations in illumination and foreground-background contrast, so effective local contrast normalization is essential for effective performance. We evaluated a several different normalization schemes. Most of them are based on clustering cells into larger spatial blocks [17] and contrast normalizing each block separately. The final descriptor is the vector of all the components of the normalized cell response from all the blocks in the detection window. We usually overlap blocks so that each scalar cell response contributes several components to the final descriptor vector, each normalized to a different block. This may seem redundant, but good standardization is critical and significantly improves performance, including overlapping. Then the performance increases by 4 percent at 10⁴ FPPW as we increase overlap from zero (stride 16) to 16-fold/4-fold linear coverage (stride 4).

We evaluated two classes of block geometries, square or rectangular, divided into grids of square or rectangular space cells, and circular blocks divided into log-polar cells. These two arrangements will be referred to as R-HOG and C-HOG (for Rectangular and Circular HOG).

Rectangular-HOG (R-HOG) blocks have several similarities to SIFT (scale-invariant feature transform) descriptors. But are used in quite a different manner. They are computed in dense grids on a single scale without dominant orientation alignment and are used as part of a larger code vector that impliedly encodes the spatial relative position to both the detection window, while scale-invariant feature transform are computed on a sparse set of scale-invariant key points, repositioned to align their powerful orientations, and used independently. Scale-invariant feature transform's are optimized for thin-wide baseline matching, Rectangular-HOG (R-HOG) dense robust spatial form coding. Other precursors include Freeman & Roth's edge orientation histograms. Usually, we use square Rectangular-HOG (R-HOG); we also tested vertical (2×1 cell) and horizontal (1×2 cell) blocks and paired descriptors, including both vertical and horizontal pairs. Vertical and vertical + horizontal pairs are significantly better than horizontal pairs on their own, but not as good as 2×2 blocks.

Our Circular HOG (C-HOG) descriptors are emblematic of Shape Contexts except that, relevantly, each spatial cell includes a stack of gradient-weighted orientation cells rather than a single orientation-independent edge-presence count [18]. The log-polar grid was initially suggested by the idea that it would allow the perfect coding of the nearby structure to be combined with the coarser coding of the wider context, and by the fact that the transformation from the visual field to the V1 cortex in primates is logarithmic. Two variants of the Circular HOG (C-HOG) geometry were evaluated, one with a single circular central cell (similar to the GLOH feature) and the other with a central cell divided into angular sectors as in shape contexts. We present results only for the circular centre variants, as they have fewer space cells than the divided centre ones and give the same performance in practice. Further details will be provided in a technical report. The layout of the Circular HOG (C-HOG) has

four parameters: the number of angular and radial bins; the radius of the central bin in pixels; and the expansion factor for the subsequent radii. At least two radial bins (centre and surround) and four angular bins (quarter) are needed for good performance. Including additional radial bins do not significantly change performance while increasing the number of angular bins reduces performance. 4 pixels is the best central bin radius, but 3 and 5 give similar results. The increase of the expansion factor from 2 to 3 leaves the performance essentially unchanged. With these parameters, neither the Gaussian spatial weighting nor the inverse weighting of cell votes by cell area changes the performance, but the combination of these two decreases slightly. These values are assumed to be fine orientation sampling. Shape contexts (1 orientation bin) require a much finer space subdivision to work well.

Block normalization operation: For each of the Histograms of oriented gradients (HOG) geometries, we evaluated four different block standardization schemes. Let v be the normalized descriptor vector, be the k -norm for $k=1, 2$, and ϵ be a small constant. The schemes are as follows:

$$L2 - \text{norm: } f \frac{v}{\|v\|_2 + \epsilon^2} \quad (8)$$

L2-Hys, L2-norm followed by clipping (limiting the maximum values of v to 0.2) and renormalizing [19]; which is to treat the descriptor vectors as probability distributions and to use the Bhattacharya distance between them. L2-Hys, L2-norm, and L1-sqrt all perform equally well, while simple L1-norm reduces performance by 5 percent and omitting normalization reduces performance by 27 percent at 10⁴ FPPW. Some regularization is needed as we evaluate descriptors densely, including empty patches, but the results are insensitive to the value over a wide range of parameters.

GLCM Features

A common statistical method for extracting textural characteristics from images was the Grey Level Co-occurrence Matrix (GLCM). Haralick identifies 14 textural features from the likelihood matrix to remotely derive the characteristics of texture statistics, in conjunction with the co-occurrence matrix. The four main characteristics of this paper are contrast; correlation, entropy, and homogeneity are shown in table 1.

Contrast: In acronym form, it is called CON. Another Comparison name is 'Sum of Square Variety. It delays the measurement of the contrast intensity between some of the pixels and the neighbour throughout the whole image.

Correlation: The correlation tests the grey levels of the adjacent pixel linear dependence. Digital Image Correlation is just an optical approach used in 2D and 3D exact estimation by image processing and imaging technique [20, 21]. The measurement of deformation, movement, strain, and optical flow is also performed in many science and engineering areas. This is commonly used. The measurement of the movement of the mouse is very normal.

Entropy: Entropy goes to show the amount of information the image requires to compress the image. Entropy aims to measure information or interaction loss in the signal transmitted and measurement of image information as well.

Homogeneity: It's called HOM in the shorter term. The value which estimates the distribution strength of elements in the Grayscale Level Co-occurrence Matrix passes to the Grayscale Level Co-occurrence Matrix diagonal. It is 1 for a Grayscale Level Co-

Table 1: GLCM Feature

Features	Description
F14	$\text{contrast} = \sum_{i,j=0}^{N-1} pij(i - j)$
F15	$\text{correlation} = \sum_{i,j=0}^{N-1} pij \frac{(i - \mu)(j - \mu)}{\sigma^2}$
F16	$\text{entropy} = \sum_{i,j=0}^{N-1} -\ln(P_{ij})P_{ij}$
F17	$\text{homogeneity} = \sum_{i,j=0}^{N-1} \frac{P_{ij}}{1 + (i - j)^2}$

occurrence Matrix diagonal and the range [0, 1]. Conversely, the homogeneities of weight values decrease exponentially with the diagonal.

In table 1, P_{ij} = symmetrical *Grayscale Level Co-occurrence Matrix (GLCM)* unit i, j standardized. N = Number for gray levels as described in the *Grayscale Level Co-occurrence Matrix (GLCM)* textures page of the Quantization Varying Properties dialog.

μ = Approximation of intensity of all pixels measured in the GLCM (Grayscale Level Co-occurrence Matrix) relationships as

$$\mu = \sum_{i,j=0}^{N-1} iP_{ij} \tag{9}$$

σ_2 = variance in the relationships leading to GLCM (Grayscale Level Co-occurrence Matrix) for all pixel reference intensities, measured as:

$$\sigma_2 = \sum_{i,j=0}^{N-1} P_{ij} (i - \mu)^2 \tag{10}$$

Classification

Convolutional Neural Network is biologically-inspired variants of Multilayer Perceptron (MLP). The Convolutional neural network comprised of various levels of layers is shown in Figure 1. Each layer has a specific kind of function. It constitutes one input and one layer of output. Multiple hidden layers can exist between these two layers. The hidden layers probably comprise convolution layers, pooling layers, and fully connected layers. Every layer's output serves as an input to the next layer is shown in table 2.

Convolution Layer: The convolution layer is a key principle in the Convolutional neural network. The primary purpose of the convolution layer is to extract low-level features from an input image. It learned the spatial relation of pixels utilizing small input data squares called filtration/kernel for learning image features. It uses a convolution operator. A filter slides over an input image. The convolution operator computes point-wise multiplication of input image pixels and filter pixels[22] and adds these multiplications to get a final number as an output. Assuming matrix is an input image and is a filtered image, it represents convolved feature. The first cell of the matrix is computed. The Convolutional neural network initializes and learns the values of these filters on its own during the training process.

Rectified Linear Unit (ReLU) Activation: An operation called

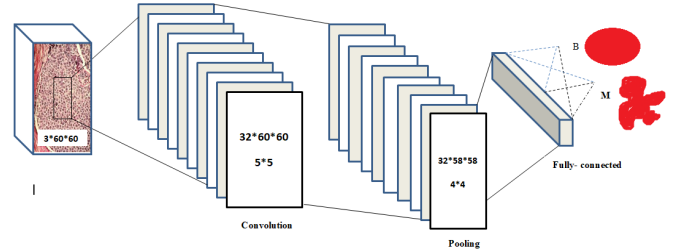


Figure 1: Proposed convolutional neural network architecture

Rectified Linear Unit (ReLU) is applied after every convolution. Rectified Linear Unit (ReLU) operation changes all negative values in the convolved image to zero and retains only positive values [23]. This introduces non-linearity in network architecture.

Average pooling: The average pooling facilitates the average calculation for every feature map patch. This means that the square is sampled for an average of 2*2 per square of the feature map.

Fully Connected Layer: It is also started calling the dense layer and a traditional MLP (Multilayer perceptron), where each neuron in the preceding layer for the next layer is connected to each neuron. At the end [24] of the architecture, the fully-connected layer is usually used to integrate the functions from underlying layers. It uses a softmax function to calculate probabilities for multiclass classification. We used binary cross-entropy as we have only two output classes

Output Layer: The Output Layer has a several neurons representing output parameters/conditions. Table 2 describes the architecture of our network. We have used two convolution layers, two max-pooling and two dropout layers [25], and one dense layer. The input is a 64x64 RGB (Red Green Blue) image and two units

Table 2: Architectural details of the proposed Convolutional neural network model

Layers	Size
Input	3*64*64
Conv1-1	32*60*60
Conv1-2	32*60*60
Avgpool 1	32*58*58
Conv2-1	32*60*60
Conv2-2	32*60*60
Avgpool 2	32*58*58
Conv3-1	32*60*60
Conv3-1	32*60*60
Avgpool3	32*58*58
Conv4-1	32*60*60
Conv4-2	32*60*60
Avgpool 4	32*58*58
Conv5-1	32*60*60
Conv5-2	32*60*60
Avgpool 5	32*58*58
Output	02

Table 3: Hardware & software Specification

Hardware & Software	Specification
RAM	Intel(R) Core(TM)i7-3.40GHz16GB
Hard Disk	1TB
Operating System	Linux
Language	Python
Front End	Spyder IDE
Back End	Image Files(Keras)

```

1776/2000 [====>...] - ETA: 1:21 - loss: 0.9502 - iou: 0.9498
1792/2000 [====>...] - ETA: 1:15 - loss: 0.9505 - iou: 0.9495
1808/2000 [====>...] - ETA: 1:09 - loss: 0.9499 - iou: 0.9501
1824/2000 [====>...] - ETA: 1:04 - loss: 0.9493 - iou: 0.9507
1840/2000 [====>...] - ETA: 58s - loss: 0.9499 - iou: 0.9501
1856/2000 [====>...] - ETA: 52s - loss: 0.9495 - iou: 0.9505
1872/2000 [====>...] - ETA: 46s - loss: 0.9493 - iou: 0.9507
1888/2000 [====>...] - ETA: 40s - loss: 0.9487 - iou: 0.9513
1904/2000 [====>...] - ETA: 34s - loss: 0.9492 - iou: 0.9508
1920/2000 [====>...] - ETA: 29s - loss: 0.9487 - iou: 0.9513
1936/2000 [====>...] - ETA: 23s - loss: 0.9484 - iou: 0.9516
1952/2000 [====>...] - ETA: 17s - loss: 0.9483 - iou: 0.9517
1968/2000 [====>...] - ETA: 11s - loss: 0.9483 - iou: 0.9517
1984/2000 [====>...] - ETA: 05s - loss: 0.9482 - iou: 0.9518
2000/2000 [====>...] - 797s 398ms/step - loss: 0.947 - iou: 0.9524 - val_loss: 0.6167 - val_iou: 0.9833
Accuracy : 0.9832773566246032
    
```

Figure 2: Convolutional neural network Result (Epoch)

2507	93
1498	52

Figure 3: Confusion matrix of Convolutional neural network

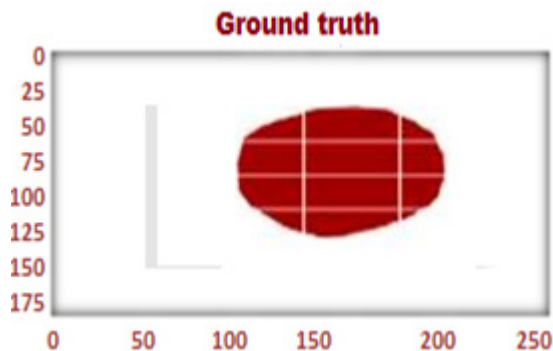


Figure 4: Ground Truth

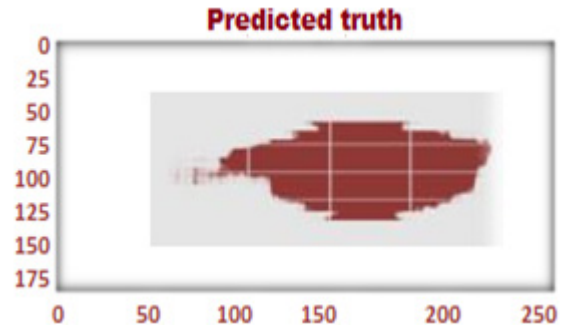


Figure 5: Predicted Truth

Table 4: Accuracy and Performance metrics of Convolutional neural network

Accuracy	Precision	Recall	F1-score	Support
98.32	91	1.00	93	2600
	09	0	07	1500

represent two skin diseases in the output layer. The convolution layer uses 32 filters of 5x5 sizes with Average pooling of size 2 x 2.

Results and Discussion

Description about Experimental Setup: After feature extraction, we move on to the image classification in of Convolutional neural network. For classification, we used a 4,100 image dataset. My laptop has not been supported for running 3,000 epochs for image classification in of Convolutional neural network. So that we got help from the Institute of Mathematical Sciences Laboratory (Research institution in Chennai, Tamil Nadu) for running my work with a High-speed efficient processor and time optimization is shown in table 3, and the Convolutional neural network classification result of the epoch is shown in figure 2, and the accuracy and performance metrics of Convolutional neural network is shown in table 4, and the confusion matrices of the Convolutional neural network classifier is shown in figure 3 and ground truth and predicated truth of the of Convolutional neural network classifier is shown in figure 4 and 5, and comparing the existing work and

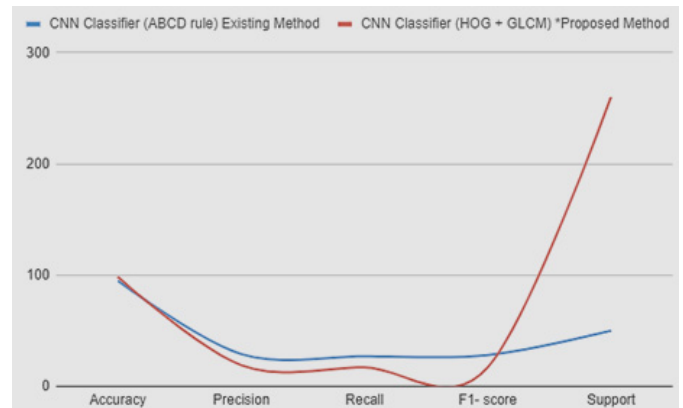


Figure. 6 Accuracy and Performance Metrics (Comparing the Existing vs. Proposed work)

Table 5: Comparing the existing and proposed work of Convolutional neural network

Metrics	CNN Classifier (ABCD rule) Existing	CNN Classifier (HOG+GLCM) *proposed
Accuracy	94.90	98.32
Precision	81.00	91.00
Recall	19.00	09.00
F1-score	99.00	93.00
	01.00	07.00
Support	500	2600
	200	1500

proposed work of Convolutional neural network in table 5, and the Accuracy and Performance Metrics (Comparing the Existing vs. Proposed work) in figure 6.

Conclusion

In this research, images of skin lesions have been segmented and classified to assist patients in detecting skin cancer without pain by cutting the infected skin. Segmentation of the Otsu algorithm functions derived from Histograms of oriented gradients (HOG) and *Grayscale Level Co-occurrence Matrix (GLCM)* was part of the diagnostic research work. The ISIC (International Skin Imaging Collaboration) dataset [12] is divided into training datasets. Training images of 2,600 were used for various kinds of benign and melanoma characteristics and evaluated with 1,550 images. A Deep convolutional neural network is used as a benign or malignant group based on the selected function to classify the skin lesion. The convolutional Neural Network outperforms in terms of precision, recall, f1-score, accuracy, as well as the predicted truth and ground truth of the skin lesion images. The positive performance of the convolutional Neural Network shows that the efficiency of the proposed technological accuracy is 98.32% and future work involves the detection of Tuberculosis Disease using the proposed process.

Acknowledgment

At the outset I thank almighty for the blessings for completing this paper in a successful manner. I wish to express the deepest gratitude to my supervisor Dr. M. Sornam M.Sc., M.C.A., Ph.D., Professor, University of Madras who wants me to achieve many things in my life and showed me a road to success by squeezing me harder and harder in this paper. Without her help, guidance, love and support this research work would have never been possible and her faith on me had made us to prove that hard work never ever fails.

References

1. S.A. Thanhakani, M. Sornam, A survey on skin classification methods using deep learning techniques skin texture analysis using machine learning, *International Journal of Research in Advent Technology*, 62-69 (2019).
2. S.A. Thangakani, M. Sornam, Skin Lesion Detection and Segmentation Using SVM and Bayesian Classification, *International journal of*

3. Computing and Algorithm, 9(1) 40-44 (2020).
3. T. Akram, H.M.J. Lodhi, S.R. Naqvi, S.R. et al., A multilevel features selection framework for skin lesion classification, *Hum. Cent. Comput. Inf. Sci.*, 10, 12 (2020).
4. A. Dutta, Md.K. Hasan, M. Ahmad, Skin lesion classification using convolutional neural network for melanoma recognition, *medrxiv.org*, 20238246 (2020).
5. S. Rashi, P. Shah, J. Bagade, Skin texture analysis using machine learning, 2016 Conference on Advances in Signal Processing, 494-497 (2016).
6. D. Priyadarshini, D. Rengini, Automatic melanoma detection using local binary pattern and support vector machine, *International Journal of Innovative Research in Computer and Communication Engineering*, 3(9), 8692-8698 (2015).
7. T. Maen, A. Abubakar, Bayesian decision fusion for enhancing melanoma recognition accuracy, 2017 International Conference on Electrical and Computing Technologies and Applications, 1-4 (2017).
8. S.L. Varma, V. Behera, Human skin detection using histogram processing and gaussian mixture model based on color spaces, 2017 International Conference on Intelligent Sustainable Systems, 116-120 (2017).
9. D.A. Shoieb, M. Sherin, W.M. Youssef, Computer-aided model for skin diagnosis using deep learning, *Journal of Image and Graphics*, 4(2), 122-129 (2016).
10. S. Kolkur, D. Kalbande, V. Kharkar, Convolution neural network for feature extraction in skin disease detection, *Journal of Advanced Research in Applied Artificial Intelligence and Neural Network*, 8-12 (2018).
11. R. Kasmi, K. Mokrani, Classification of malignant melanoma and benign skin lesions: implementation of automatic ABCD rule, *IET Image Processing*, 10(6), 448-455 (2016).
12. <http://www.isdis.net/index.php/isis-project>
13. P. Dubal, S. Bhatt, C. Joglekar, S. Patil, Skin cancer detection and classification, *International Conference on Electrical Engineering and Informatics*, 1-6 (2017).
14. M. Esole, P. Jefferson, M.J. Kang, Euler characteristics of crepant resolutions of Weierstrass models, *Communications in Mathematical Physics*, 371, 99-144 (2019).
15. R. Mishra, O. Daescu, Deep learning for skin lesion segmentation, *International Conference on Bioinformatics and Biomedicine*, 1189-1194 (2017).
16. W. Zhou, G. Shengyu, L. Zhang, X. Lou, Histogram of oriented gradients feature extraction from raw bayer pattern images, *Transactions on Circuits and Systems II*, 67(5), 946-950 (2020).
17. S. Swarnima, D. Singh, V.Y. Singh, Face recognition using HOG feature extraction and SVM classifier, *International Journal of Emerging Trends in Engineering Research*, 8(9), 6437- 6440 (2020).
18. I.F. Sudirman, H.G. Winda, P.S. Intan, S. Ndraha, I. Fawwaz, Linear kernel and polynomial analysis in recognizing tuberculosis image using HOG feature extraction, *Journal Mantik*, 1693-1698 (2020).
19. Putra, FAI Achyunda, F. Utaminigrum, F.M. Wayan, HOG feature extraction and KNN classification for detecting vehicle in the highway, *Indonesian Journal of Computing and Cybernetics System*, 14(3), 231-242 (2020).
20. H. Fan, F. Xie, Y. Li, Z. Jiang, J. Liu, Automatic segmentation of dermoscopy images using saliency combined with Otsu threshold, *Computers in Biology and Medicine*, 85, 75-85 (2017).
21. K.C. Tatikonda, M.B. Chandra, K.S. Srinivas, The analysis of digital mammograms using HOG and GLCM features, *International Conference on Computing, Communication and Networking Technologies*, 1-7 (2018).
22. W. Sheng-Yu, O. Wang, R. Zhang, A. Owens, A.A. Efros, CNN-generated images are surprisingly easy to spot... for now, *Conference on Computer Vision and Pattern Recognition*, 8695-8704 (2020).
23. G. Fatima, Skin cancer diagnosis by using fuzzy logic and GLCM, *Journal of Physics Conference Series*, 012020 (2019).
24. P. Tri-Cong, L. Chi-Mai, M. Visani, H. Van-Dung, Deep CNN and data augmentation for skin lesion classification, *Asian Conference on Intelligent Information and Database Systems*, 573-582 (2018).
25. K. Jeremy, G. Hamarneh, Multi-resolution-tract CNN with hybrid pretrained and skin-lesion trained layers, *International workshop on machine learning in medical imaging*, 164-171 (2016).